

Preliminary investigation of the impact of polymer composition on electrochemical properties of coatings as determined by electrochemical impedance spectroscopy

Vinod Upadhyay, Umesh D. Harkal, Dean C. Webster,
Gordon P. Bierwagen

© American Coatings Association & Oil and Colour Chemists' Association 2013

Abstract The influence of structural and systematic compositional variations in glycidyl carbamate (GC) functional polymers on the electrochemical properties of their coatings was studied. There are few reports which focus on the correlation of structural and compositional variations in polymer films with their electrochemical barrier properties, diffusion properties with regards to water and aqueous electrolytes, and corrosion performance. To begin to fill this knowledge gap, two sets of GC functional polymers were studied. The polymer compositions were designed to vary the extent of polar hydrophilic groups, non-polar hydrophobic groups, and reactive epoxy groups in the final coatings. Impedance responses of the coatings were found to be closely related to the structural and compositional variations of these GC polymer films. In addition, single frequency EIS experiments were used in an attempt to understand the water uptake behavior of these polymer films using NaCl solution and ionic liquid under immersed condition. The resulting transport property data of the films was correlated to their polymer structure and composition. Moreover, a novel attempt at ranking the stability of coating using capacitance measurement during a cyclic wetting–drying condition was also attempted. The information obtained from this work can potentially be used to optimize the polymer for the specific performance properties needed in the protective coat-

ing applications, saving significant time and effort in the research and development stage.

Keywords Polymer, Coating, Structure–property relationship, Electrochemical impedance spectroscopy, Stability ranking

Introduction

Organic coating films are widely used as barriers to the transport of oxygen, ions, and electrolytes from the environment to prevent materials from corrosion and other forms of degradation, as well as imparting aesthetic appearance and specialty functions.¹ In their final film form they consist primarily of a polymeric binder and pigments plus additives. The binder, to a large extent, governs the transport and mechanical performance properties of the coating. Various binders such as polyurethanes, epoxies, acrylics, drying oils, alkyds, polyesters, silicones, phenolic, and amines are used in the coating industries.²

Two of the most important high performance coating systems currently in use are polyurethanes (PU) and epoxies. PU are widely used due to their superior properties, such as high gloss, chemical resistance, and acid etch resistance. An added advantage of PU coatings is their ability to form strong hydrogen bonds, thus enhancing coating film performance and physical properties such as abrasion resistance and film toughness. Films formed from epoxy systems exhibit good corrosion performance, wetting of metals, adhesion, chemical resistance, strength, and toughness.^{3,4} A novel way of achieving the advantage of both PU and epoxy systems is to unite them by the use of glycidyl carbamate (GC) chemistry which utilizes both urethane linkages and reactive epoxy groups.^{5–7}

V. Upadhyay, U. D. Harkal, D. C. Webster,
G. P. Bierwagen
Department of Coatings and Polymeric Materials, North
Dakota State University, Fargo, ND 58102, USA

Present Address:

V. Upadhyay (✉)
Chemical and Biomolecular Engineering, University
of Akron, Akron, OH 44304, USA
e-mail: vinod@uakron.edu

Changes in the polymer structure and composition are expected to change the final properties of the coating films such as glass transition temperature, hardness, flexibility, toughness, barrier, and diffusion. In a recent work, Devenci et al.⁸ chemically modified polystyrene with succinic anhydride and phthalic anhydride and observed that the modified polymer displayed better thermal, mechanical, elastic, and corrosion resistance properties. The corrosion performance, however, was only characterized by visual observation. A study of the influence of plasticizer composition variation on the performance of an epoxy coating as measured by electrochemical impedance spectroscopy (EIS) has also been reported.⁹ It is also well known that up to 6% water can be absorbed in epoxy coatings, and this drastically affects the thermal behavior of the coatings and their electrochemical barrier properties. Li et al.¹⁰ have written an extensive analysis of thermal (and aqueous) effects on electrochemical properties of organic coatings that reviewed the literature through 1997.^{11,12}

These studies outline the manner in which electrochemical properties are affected by polymer variations and the variations in temperature and water content in the polymer. However, investigations of the influence of systematic polymer structural and compositional variations on the EIS response of coated systems are entirely absent or, at best, incomplete. EIS is a very powerful technique and is widely used to study the protective properties of organic coatings on corrodible materials.^{13–17} It can also allow for the determination

of the failure mechanism and water uptake behavior of the coating.^{18–21}

The aim of this work is to investigate the influence of systematic polymer structural and compositional variations on the electrochemical properties of unpigmented coating films as measured by EIS. Novel thermosetting GC functional polymers were designed with structural as well as compositional variations. The designed polymers were then cured with amine cross-linkers. EIS measurements were performed on the cured coating systems and the influence of polymer structural and compositional variation on the EIS response was investigated. The effect of such changes on the absorption and desorption behavior of water was also studied.

Experimental

Of the eight coating films studied in this work, five were based on modified branched GC polymers, termed M series GC resins, and synthesized using hexamethylene diisocyanate biuret (HDB) polyisocyanate, alcohols, and glycidol. The remaining three films were based on linear GC polymers and were labeled L series GC resins. Both M and L series coatings were solvent-based systems.

In general, GC functional resins are obtained by the reaction of glycidol with an isocyanate functional compound, as shown in Fig. 1. This polymer system has the unique property of having both epoxy and

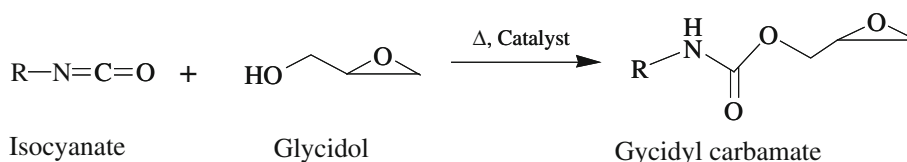


Fig. 1: Schematic representation of the synthesis of GC functional resins

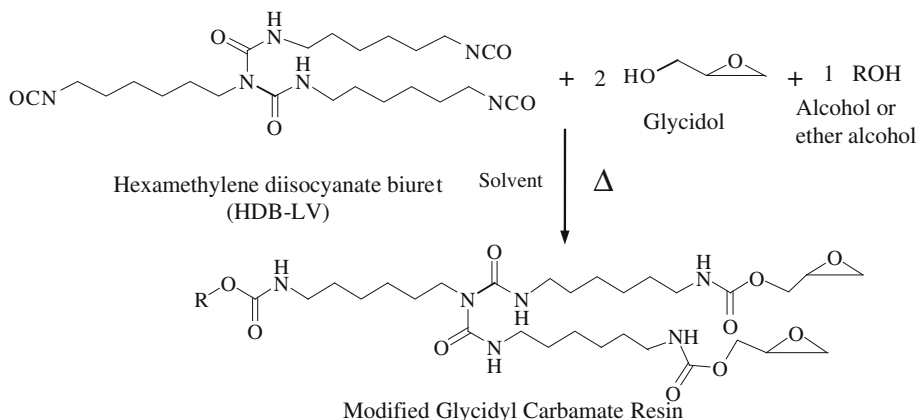
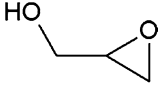
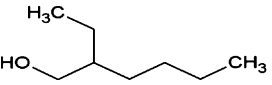
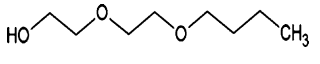
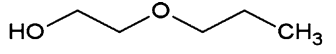
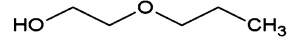
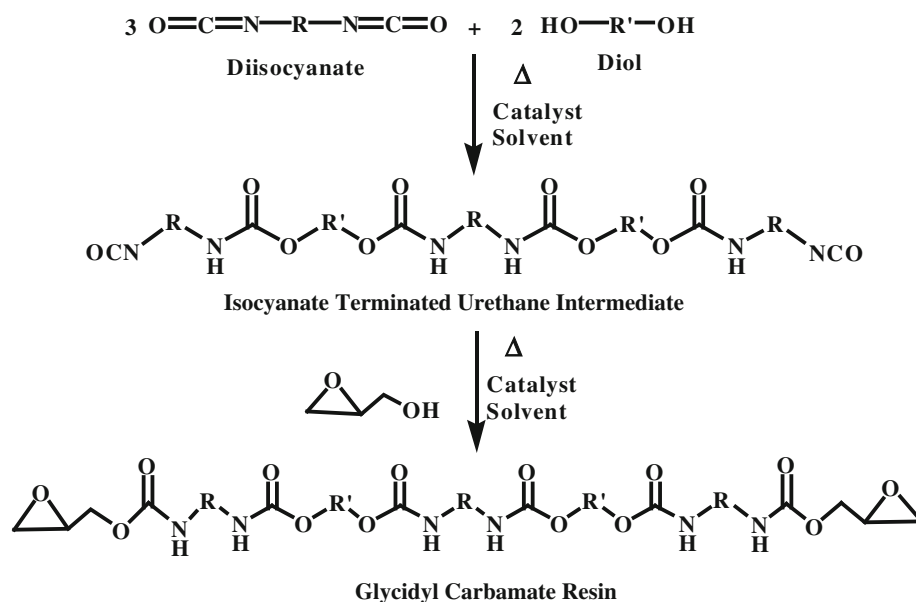


Fig. 2: Schematic of M series GC resin synthesis

Table 1: Compositions of the M series GC resins

Name of R'OH	Structure of R'OH	Corresponding GC polymer	NCO:glycidol:alcohol/ether alcohol (molar ratio)	EEW (gm/eq)
Glycidol		BGC	1:1:0	255
2 Ethyl hexanol (2EHA)		BGC-2EHA	1:0.66:0.33	450
Diethyleneglycol butylether (DB)		BGC-DB	1:0.66:0.33	384
Ethyleneglycol propylether (EP)		BGC-EP	1:0.66:0.33	355
Ethyleneglycol propylether (EP)		BGC-EP (15%)	1:0.85:0.15	336

The polyisocyanate used was HDB in all cases

**Fig. 3: Schematic of L series GC resin synthesis**

urethane functional groups in its structure, thereby combining the reactivity of epoxides and the performance of urethanes in a single polymer structure.⁵⁻⁷

M series GC resins

The details of the synthesis and characterization of the M series GC polymers has been reported in prior work by Harkal et al.⁷ As illustrated in Fig. 2, HDB polyisocyanate was reacted with an equivalent amount of glycidol alone or in combination with an alcohol/ether alcohol to obtain the M series GC resins. Table 1

lists the details of the M series GC resins. Among the five M series GC resin compositions, one of the compositions was based on HDB and glycidol at stoichiometric equivalents of isocyanate to hydroxyl at the ratio 1:1 (–NCO:–OH) and was named biuret glycidyl carbamate (BGC) resin. Three compositions were obtained by replacing 33 mol% of glycidol with an alcohol or an ether alcohol, keeping the equivalent ratio of isocyanate, glycidol, and alcohol/ether alcohol at 1:0.66:0.33 or 3:2:1 (NCO:glycidol:alcohol/ether alcohol). The remaining fifth composition was obtained by replacing 15 mol% glycidol by ethyleneglycol propylether.

Table 2: Compositions of the L series GC resins

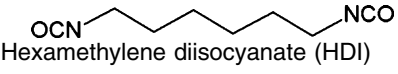
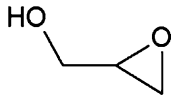
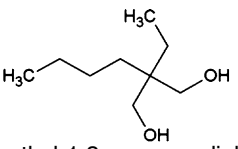
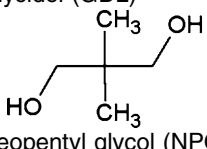
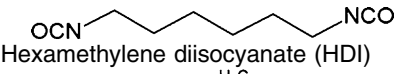
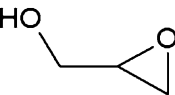
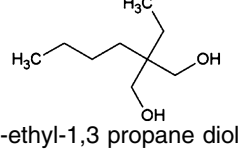
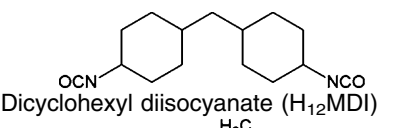
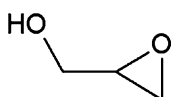
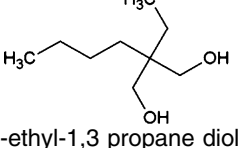
Polymer (molar ratio)	Composition	EEW	
L-A HDI–BEPD–NPG–GDL (1:0.33:0.33:0.33)	 Hexamethylene diisocyanate (HDI)	 Glycidol (GDL)	510
	 2-Butyl-2-ethyl-1,3 propane diol (BEPD)	 Neopentyl glycol (NPG)	
L-B HDI–BEPD–GDL (1:0.66:0.33)	 Hexamethylene diisocyanate (HDI)	 Glycidol (GDL)	502
	 2-Butyl-2-ethyl-1,3 propane diol (BEPD)		
L-C H ₁₂ MDI–BEPD–GDL (1:0.66:0.33)	 Dicyclohexyl diisocyanate (H ₁₂ MDI)	 Glycidol (GDL)	681
	 2-Butyl-2-ethyl-1,3 propane diol (BEPD)		

Table 3: Properties of L series GC resins

L series GC polymers	EEW (gm/eq)	Wt% Non-polar hydrocarbon in polymer composition
L-A	510	58.0
L-B	502	57.8
L-C	681	65.0

L series GC resins

All the three L series GC resin formulations were based on diisocyanates, diols, and glycidol. The synthesis of these polymers was a two-step reaction process, as shown in Fig. 3. In the first step, a diisocyanate terminated urethane intermediate was formed by the reaction of an excess of diisocyanate and diol(s), and in the second step glycidol was added to obtain the GC resins. Details of synthesis and characterization are described in detail elsewhere.²² The three L series GC resin were labeled as L-A, L-B, and L-C and had epoxy equivalent weights of 510, 502, and 681, respectively. Tables 2 and 3 list their compositions and properties.

Coating preparation and film formation

Details of coating film preparation for the M series GC resins-based coating system have been described elsewhere.⁷ Briefly, the prepared polymers were crosslinked with a polyamide, Ancamide 2353. The ratio of amine active hydrogen to epoxy equivalents was kept at 1:1 for all the coating formulations. The coatings films were then drawn down on steel panels (Q-Panel, 0.5 × 76 × 152 mm) which had been cleaned with *p*-xylene and cured at 80°C for 1 h and 45 min and then kept at ambient conditions for 3 days prior to the EIS experiments. Dry film thicknesses of about 80–85 μm were prepared. The coating films were then labeled M1, M2, M3, M4, and M5 obtained from polymers BGC, BGC-2EHA, BGC-DB, BGC-EP, and BGC-EP (15%), respectively. For the L series GC resin-based coating system, Ancamide 2353 was also the crosslinker used and the coatings were prepared as above. The coatings were cured in an oven at 80°C for 1 h and kept at room temperature for 2 weeks before the EIS measurements were performed on them. Coatings were labeled L1, L2, and L3 based on GC resins L-A, L-B, and L-C, respectively.

Electrochemical impedance spectroscopy measurements

A Gamry Instruments R 600 Potentiostat/Galvanostat/ZRA in conjunction with Gamry Framework Version 5.20/EIS 300 software was used for the EIS experiments. The instrument was purchased from Gamry Instruments, Inc. of Willow Grove, PA. A Perspex™ cylinder with a surface area of 7.07 cm² was mounted on the samples and was clamped with an O-ring insert to facilitate electrochemical measurements. Sufficient electrolyte was filled in the cylinder to aid EIS measurement.^{12,23,24}

Two types of EIS measurements were performed. One was multifrequency EIS (MF-EIS). A schematic of the MF-EIS set-up is shown in Fig. 4. The MF-EIS set-up consists of metal substrate as the working electrode (WE) with Platinum (Pt) and saturated calomel electrode (SCE) as counter and reference electrodes, respectively. The electrolyte used for the experiment was 5 wt% NaCl, also used in the B117 salt spray test. Information about the coating performance, failure mechanism, and various processes involved can be derived via MF-EIS. The impedance response corresponding to the applied frequency of 10⁵ to 10⁻² Hz was measured with an acquisition rate of 10 points per decade. A 10 mV amplitude perturbation potential with respect to the open circuit potential was used during the measurement.²⁴

The other EIS performed was single frequency EIS (SF-EIS) measurement, where the capacitance response of the coating at an applied frequency of 10⁴ Hz was monitored every 30 s. The equation $C = -\frac{1}{2\pi fZ''}$ was used to calculate the capacitance from the measured impedance data, where C is the capacitance, Z'' is the imaginary component of the measured impedance, and f is the frequency of measurement. At very high frequency of measurement, Z'' contains little resistance information and will be stationary,¹³ with a high signal to noise ratio because of the sampling rate. By SF-EIS capacitance measurements, water ingress from an aqueous electrolyte, water egress into a hydrophilic ionic liquid and diffusion behavior of the coating have been studied based on the high dielectric constant of water vs the low dielectric constant of the polymers.^{25,26} Varying polymer structure and composition is expected to vary the SF-EIS response of the coating with certain signatures distinguishing one coating film from another. SF-EIS measurements were performed in this experiment for both the wetting and the drying stage of the coating. The wetting stage consisted of monitoring the capacitance of the coating continuously for 48 h in 5 wt% NaCl immersed condition and has the same set-up as in Fig. 4; whereas the drying stage was capacitance measured with a hydrophilic room temperature ionic liquid (RTIL) as electrolyte.²⁷ The RTIL used was 1-butyl-1-methylpyrrolidinium trifluoromethanesulfonate (C₁₀H₂₀F₃NO₃S) (procured from EMD chemicals, Inc. of Gibbstown NJ). This RTIL is hydrophilic and can cause a coating

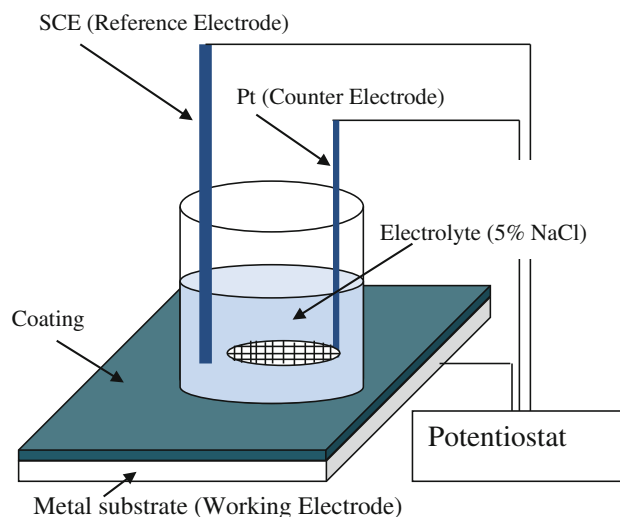


Fig. 4: Schematic of three-electrode EIS set-up

to dry. Thus the drying process can be followed by SF-EIS. The drying step was also monitored for 48 h. A two-electrode electrochemical cell was used for the drying stage SF-EIS test with substrate as the working electrode and Pt mesh as the counter/reference electrode.^{27,28}

Results and discussion

M series GC coatings: electrochemical characterization

The measurement of water uptake by a capacitance measurement on a coating film is based on the assumption that the change in capacitance of the film after immersion of the film in an aqueous electrolyte is due to the uptake of water by the film. The Brasher-Kingsbury equation, $\Phi_v = \frac{\log(C_t/C_0)}{\log(80)}$ relates the water uptake by a coating to the coating capacitance where Φ_v is the volume fraction of absorbed water, C_t and C_0 are the coating capacitance at any time t and at time $t = 0$, respectively, and 80 is the dielectric constant of water.²⁹ The coating capacitance can be written as $C = \frac{\epsilon\epsilon_0 A}{d}$, where ϵ is the relative dielectric constant of the coating, ϵ_0 is the dielectric constant of vacuum, A is the area of the coating, and d is the coating thickness. Organic polymers have dielectric constants values of around 3–5, whereas the dielectric constant of free water is around 80.³⁰ Permeation of water into an organic coating film therefore results in an increase in the dielectric constant of the coating film and, in the process, increases the capacitance of the coating. A change in the relative dielectric value of the coating can be directly measured from the change in capacitance of the coating film, if there is no significant change in thickness. The imaginary impedance Z'' as measured by EIS can furnish information about the capacitance of a coating, and as such, furnish

information about the water uptake behavior of the coating. EIS for capacitance measurement was performed at 10^4 Hz to ensure that the system is relatively stationary with respect to the measurement.^{13,31} Capacitance values were obtained from the SF-EIS imaginary impedance (Z') data for all the coating films under investigation. The diffusion coefficients during wetting and drying steps were obtained according to the mathematical equations of diffusion described elsewhere.^{32,33} Many other authors have also considered such measurements as applied to coatings.^{34–38}

An influence of structural modification as well as polymer composition on the single frequency capacitance behavior of M series GC resins is observed in Fig. 5. The trend in capacitance at saturation during the wetting stage is $M3 > M1 > M4 > M5 > M2$. A direct comparison between coatings M2, M3, and M4 can be made. They differ only in the structure of the alcohol used, each being 33 mol%, as seen in Table 1. The coating based on BGC-DB (M3) contained the most hydrophilic, two ether groups in its alcohol structure, whereas BGC-2EHA (M2) contained the most hydrophobic of the three, with no hydrophilic ether groups. BGC-EP (M4) contained more hydro-

philicity than M2 but less than M3. The capacitance trend observed for the three is therefore consistent with the hydrophilicity of the alcohol groups used, with M3 displaying the maximum water absorption and M2 displaying the least. Similar comparison can be made between M4 and M5. M4 contains higher composition of ether alcohol compared to M5 for similar ether alcohol structure as observed from Table 1. Higher composition of ether results in higher water uptake as observed for M4 compared to M5. Therefore, an effect of both the resin structure and monomer composition on the water uptake behavior is observed.

Similar trends as observed for the water uptake behavior were also seen for the diffusion behavior of the M series GC resins in their wetting stage, as observed in Fig. 6a. Diffusion coefficient values were calculated using the methods of Allahar et al.^{26,32} M1, M2, M3, M4, and M5 displayed a diffusion coefficient value of 3.97×10^{-13} , 2.66×10^{-13} , 8.88×10^{-13} , 4.08×10^{-13} , and $4.63 \times 10^{-13} \text{ m}^2/\text{s}$, respectively. Among M2, M3, and M4, M3 displayed the maximum rate of water uptake, whereas M2 displayed the lowest,

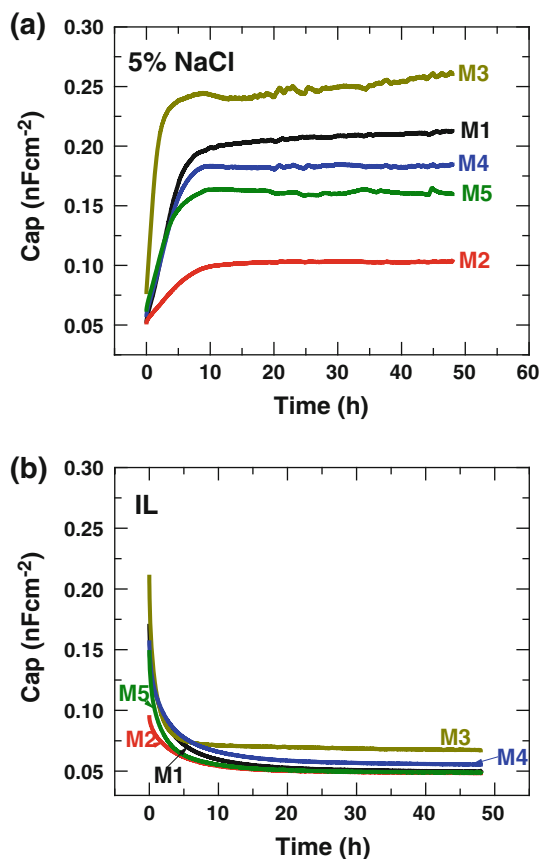


Fig. 5: Capacitance results for M series GC based coatings as a function of immersion time for samples M1, M2, M3, M4, and M5 in (a) 5 wt% NaCl for (b) in room temperature ionic liquid

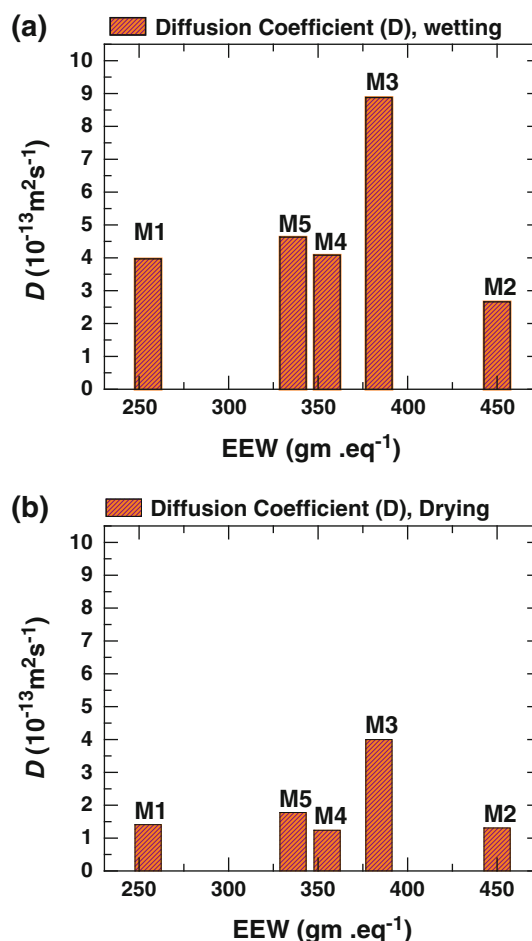


Fig. 6: Dependence of diffusion coefficient on EEW concentration in polymer for M series coatings during (a) wetting cycle and (b) drying cycle

and M4 displayed a value in between. This is also consistent with the hydrophilicity and hydrophobicity of the three coatings, with the most hydrophobic (M2) displaying the lowest diffusion coefficient value, indicating that the diffusion rate can be controlled by the structure of the polymer. Between M4 and M5, with the change in the composition of ether group, the trend as expected was not observed. Perhaps the slight difference in ether composition between M4 and M5 was not significant enough to effect a change in the diffusion coefficient value to the accuracy of the measurements.

Diffusion coefficients measured during RTIL assisted drying are shown in Fig. 6b. Values obtained for M1, M2, M3, M4, and M5 were 1.41×10^{-13} , 1.31×10^{-13} , 4.0×10^{-13} , 1.24×10^{-13} , and 1.78×10^{-13} m²/s, respectively. Similar to the wetting stage, the diffusion coefficient measured for the drying stage was highest for M3, indicating that the drying rate could be controlled by structure manipulation. However, the overall diffusion trend during drying was not similar to the wetting state, as observed in other studies.^{25,26}

On further observation and comparison of Figs. 6a and 6b, it is seen that the diffusion coefficient value during the wetting stage was greater than the diffusion coefficient value during the drying stage. This observation is consistent with the trend observed for epoxy systems. It is believed that the local drying of the interface during the initial drying step would lower the

global or average diffusion coefficient by locally slowing interfacial transport, and plasticization of the coating would increase the diffusion coefficient of the coating during the wetting step by locally increasing interfacial transport.^{25,26}

MF-EIS measurement performed for the M series samples is shown in Fig. 7. An initial EIS spectrum was obtained just after immersion to ensure a defect-free coating. Bode modulus and phase angle plots for all M series coatings are shown. Considering that this type of coating is often modeled as a capacitor and resistor in parallel, and assuming a negligible solution resistance, the impedance of a coating can be written as

$$|Z| = \frac{1}{\frac{1}{R} + j\omega C}$$

where $|Z|$ is the impedance, R is the resistance of the coating, C is the capacitance of the coating, and ω is the angular frequency of measurement. At low frequency the impedance is dominated by the resistive component and is a measure of coatings resistance. A coating with $|Z|_{0.01 \text{ Hz}}$ value less than $10^6 \Omega \text{ cm}^2$ is often believed to indicate poor barrier performance.^{20,39,40}

An analysis of the Bode plot in Fig. 7 at 2 h and at 7 days of immersion reveals interesting results. On comparing coatings M2, M3, and M4, coating M2 with the most hydrophobic alcohol structure displayed the

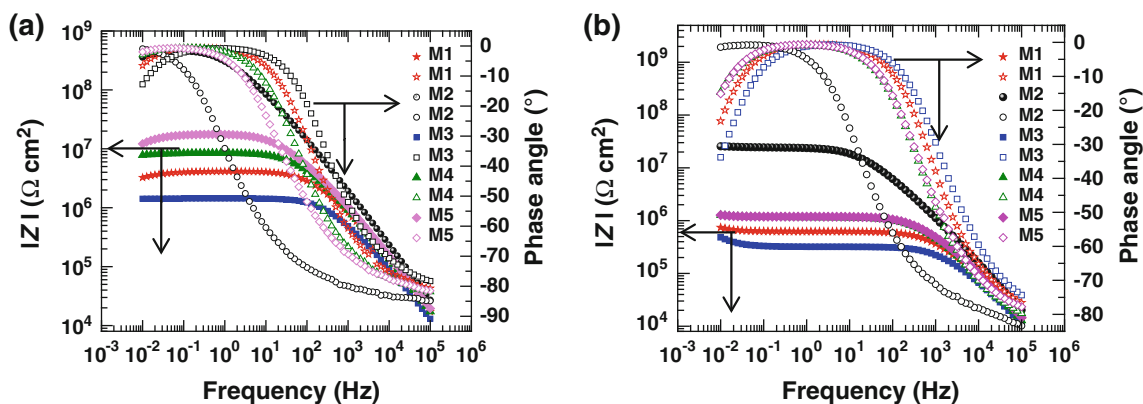


Fig. 7: Bode plot of M series GC polymer-based coating after (a) 2 h of constant immersion and (b) 7 days of constant immersion

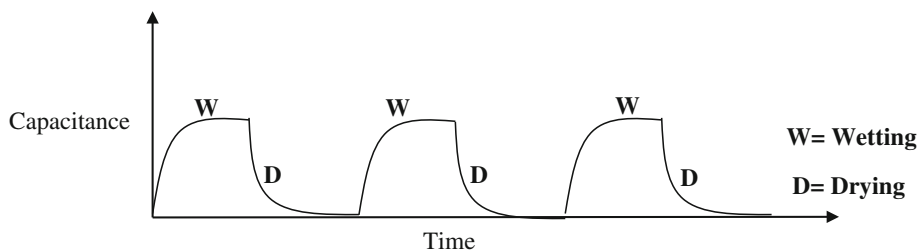


Fig. 8: Schematic of the expected capacitance during cyclic wetting–drying process

highest impedance of the three, whereas M3, with the most hydrophilic ether, displayed the lowest impedance. On comparing coatings M4 and M5, a minor increase in impedance is observed for coating M5 compared to M4. Coatings M4 and M5 have a similar polymer system except that the polymer composition in M5 has a slightly lower content of the hydrophilic ether group compared to system M4, as shown in Table 1. A similar trend, but with a decrease in the

$|Z|_{0.01\text{ Hz}}$ values for all the coating systems was observed at day 7 with superimposition of Bode plots for M4 and M5. This indicates that the slight compositional differences in ether groups in M4 and M5 were not sufficient to bring significant change in impedance after 7 days.

The trend in low frequency impedance ($|Z|_{0.01\text{ Hz}}$) behavior of the M series coatings is also observed to correlate with the EEW, although not completely. M2

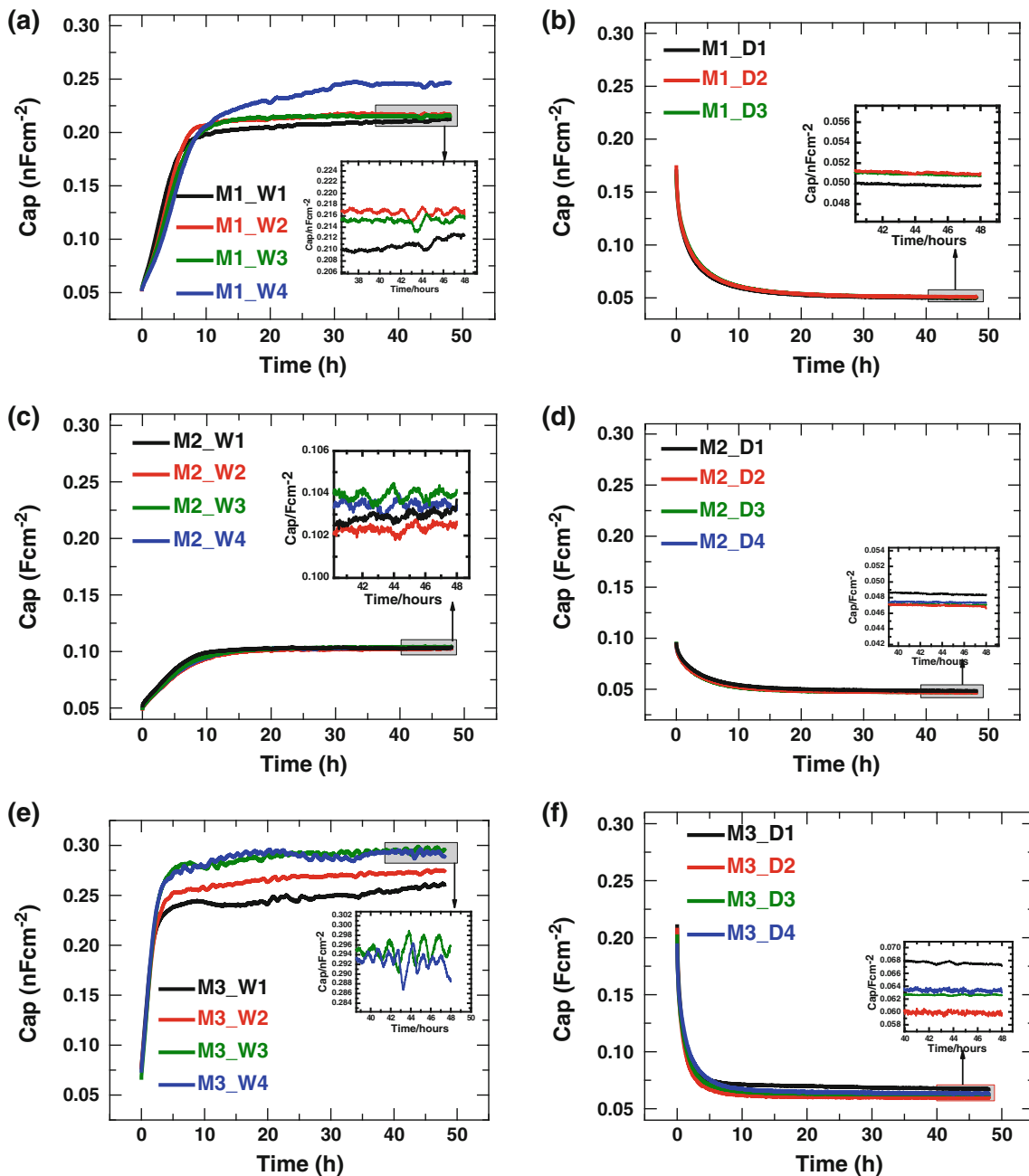


Fig. 9: Cycles of capacitance as a function of immersion time for coatings (a) M1 during wetting, (b) M1 during drying, (c) M2 during wetting, (d) M2 during drying, (e) M3 during wetting, (f) M3 during drying, (g) M4 during wetting, (h) M4 during drying, (i) M5 during wetting, and (j) M5 during drying. Some portions are magnified only to facilitate distinction of plots. However, comparison among the magnified regions cannot be made since their scales are different

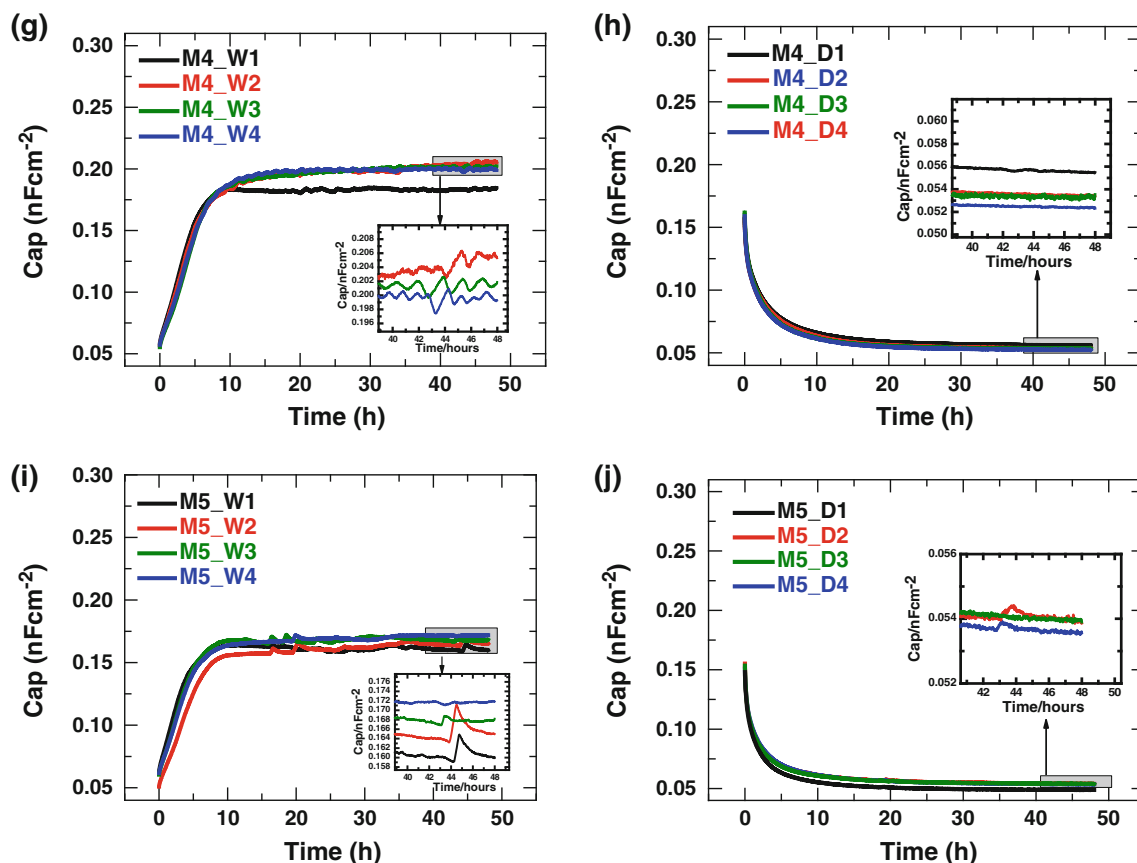


Fig. 9: continued

has the highest EEW and displayed maximum $|Z|_{0.01 \text{ Hz}}$. Lower EEW resins require a higher amount of amine crosslinker and can be expected to generate more of polar tertiary amines and hydroxyl groups in the coatings during crosslinking compared to the coatings obtained from higher EEW polymers. Hence, higher $|Z|_{0.01 \text{ Hz}}$ values can be expected from higher EEW polymers.

Coating stability characterization by single frequency EIS

In an attempt to investigate the further utility of SF-EIS in ranking the stability of coating systems by capacitance measurement under wetting–drying conditions, cyclic SF-EIS was performed on all five M series coating films. Stability, as defined in this work, corresponds to when the coating film does not show a change in capacitance under cyclic wetting–drying condition. Cyclic SF-EIS capacitance measurements consisted of a wetting cycle under constant immersion conditions in 5 wt% NaCl for 48 h, followed by drying (desorption) of the absorbed electrolyte by a hydrophilic ionic liquid for the next 48 h. The drying step was followed again by a wetting step, and so on. Four

cycles were run for all samples. Figure 8 is a schematic of the expected capacitance change during the cyclic wetting–drying process.

Figures 9a, 9c, 9e, 9g, and 9i correspond to the capacitance of the wetting cycles, whereas Figs. 9b, 9d, 9f, 9h, and 9j correspond to the capacitance of the drying cycle for all the samples. M1_W1 (Fig. 9a) corresponds to the capacitance of the first wetting cycle of coating M1. This was followed by the capacitance measurement of the first drying cycle in ionic liquid M1_D1 (Fig. 9b). M1_W2 corresponds to the second wetting cycle, which was followed by M1_D2 of the drying step, and so on, as shown in the schematic. For sample M1, the sample failed prior to M1_D4 and hence is not plotted.

An examination of the plots reveals interesting information about the stability of the coating. The trend in the capacitance behavior for all the coatings during the drying steps for all the cycles is similar. During the wetting stages, samples M2 and M5 did not display any change in capacitance behavior for all the wetting cycles. However, changes in the capacitance behavior in the wetting stages were observed for samples M1, M3, and M4. Up to cycle 3 coating, M1 did not display any change in capacitance. An increase in capacitance was observed during cycle 4. For coating

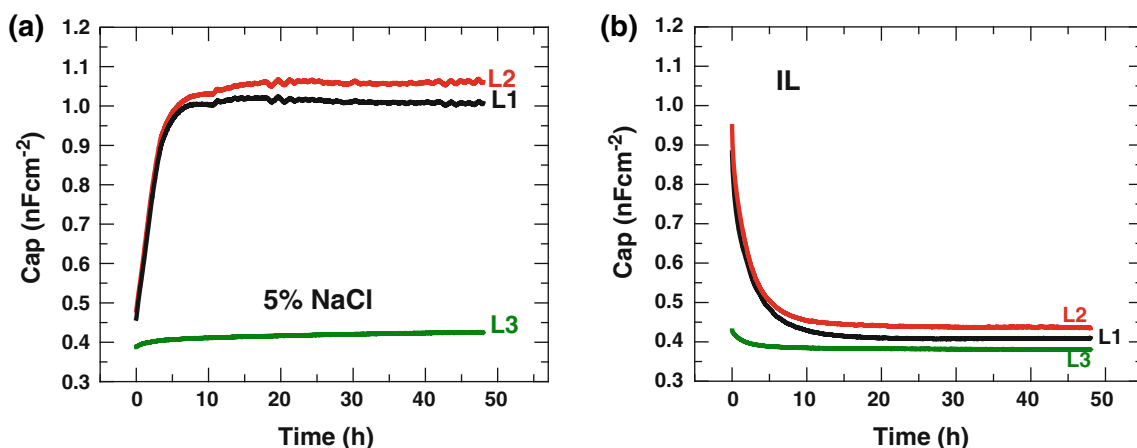


Fig. 10: Capacitance results for L series GC-based coatings as a function of immersion time for samples L1, L2, and L3 at (a) 5 wt% NaCl and (b) in room temperature ionic liquid

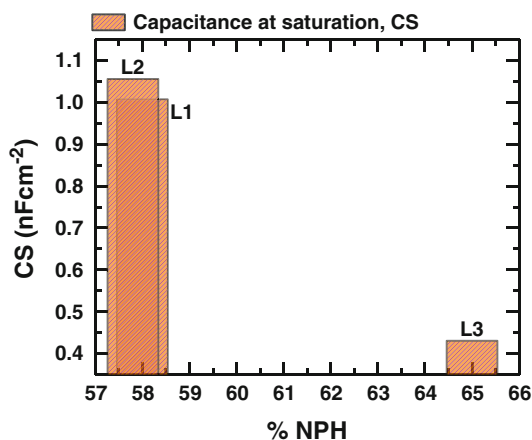


Fig. 11: Capacitance at saturation as a function of wt% NPH for L series samples

M3, an increase in capacitance was observed during cycle 2 and a further increase was observed during cycle 3. Cycle 4 displayed similar capacitance compared to cycle 3. For coating M4, cycle 2, cycle 3, and cycle 4 displayed similar but increased capacitance behavior compared to cycle 1. Such change in the water uptake behavior for samples M1, M3, and M4 indicates progressive and irreversible changes in the dielectric behavior of the coating, which could be due to changes in polymeric structure, formation of new product, or changes in molecular orientation in the coating during wetting.

On comparing the alcohols used in the M series coatings, coating M2 was formulated with no hydrophilic groups, whereas coating M5 was formulated with 15% ethyleneglycol propylether. The coating systems M3 and M4 had an increased amount of hydrophilic content, as shown in Table 1. The higher fraction of hydrophilic groups in M3 and M4 might be responsible for causing higher water absorption and plasticization

Table 4: Diffusion coefficient of coatings L1, L2, and L3 during wetting and drying

Coating	Diffusion coefficient, wetting stage $\times 10^{-13} \text{ m}^2/\text{s}$	Diffusion coefficient, drying stage $\times 10^{-13} \text{ m}^2/\text{s}$
L1	6.24	2.03
L2	6.15	2.69
L3	0.94	2.49

of the polymer films causing capacitance changes.^{13,41} M2 and M5 displayed no capacitance change compared to M1, M3, and M4, and the coatings films were relatively stable and resisted change. The utility of SF-EIS capacitance measurement in ranking the stability of coating is well demonstrated by the data.

L series GC coatings: electrochemical characterization

A comparison of the capacitance measurements during wetting and drying steps for the L series GC resins can be seen in Fig. 10. It is observed that the film from L3, the most hydrophobic polymer, displayed the least capacitance during both the wetting and drying stage compared to samples L1 and L2. L1 and L2 display similar capacitance. As seen in Table 2, L3 polymer consists of a rigid cycloaliphatic isocyanate in contrast to the flexible aliphatic isocyanate for L1 and L2. The negative impact of the hydrophobic nature of the polymeric structure on the water uptake behavior is clearly shown.

The capacitance trend displayed is also observed to have a direct correlation with the wt% non-polar hydrocarbon (NPH) content in the coating, as seen in Table 3. Coating L3 with the highest NPH (65 wt%) displayed the lowest capacitance compared to coatings

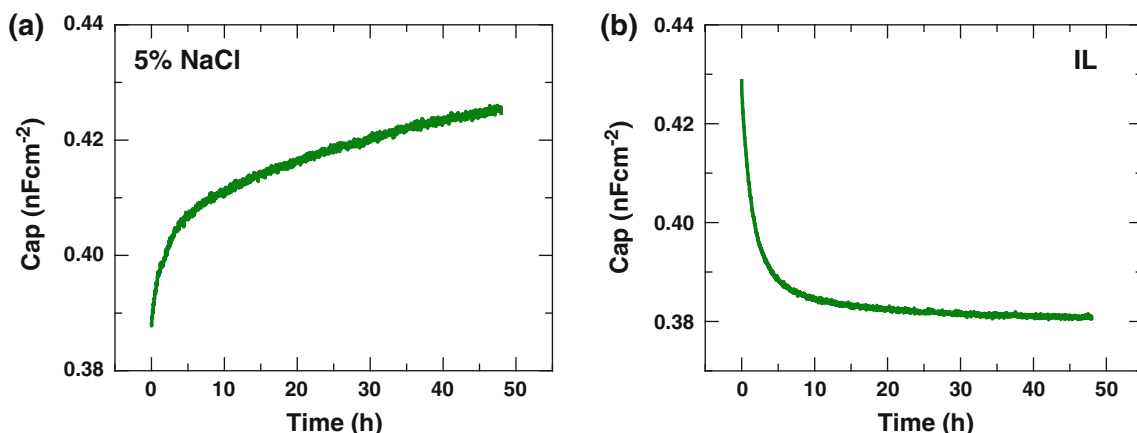


Fig. 12: Capacitance evolution with time for coating L3 during (a) wetting and (b) drying

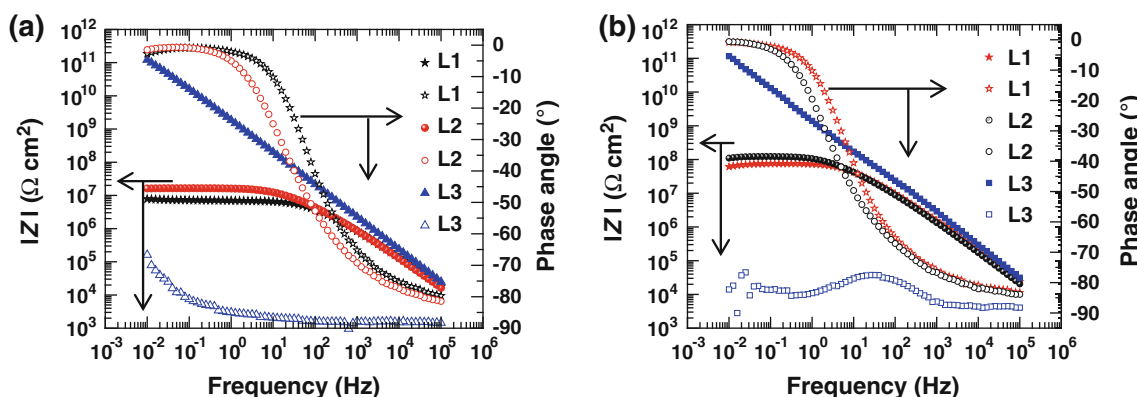


Fig. 13: EIS Bode plots for coatings L1, L2, and L3 after (a) 2 h and (b) 7 days constant immersion in 5 wt% NaCl

Table 5: Wet and dry T_g of L coatings

Coatings	Dry T_g (°C)	Wet T_g (°C)
L1	20	1
L2	18	9
L3	57	45

L1 and L2, as observed in Fig. 11. Higher NPH content in the coating resists the aqueous electrolyte absorption and hence reduces water uptake, as shown in the capacitance plots.

Values of the diffusion coefficient for the L series coatings for wetting and drying are shown in Table 4. As observed, the diffusion coefficient value of the wetting step is higher than the drying step for L1 and L2. However, an anomaly is observed for L3. The D value for L3 during wetting is lower compared to drying. The D values were calculated based on the assumption that the diffusion is Fickian and saturation is reached. However, on observation of Fig. 12 it is shown that L3 does not reach saturation during the

time of the immersion (48 h) in aqueous electrolyte. Saturation of coating is a requirement for the calculation of the diffusion coefficient.

Figure 13 displays the Bode modulus along with the phase angle plot for coatings L1, L2, and L3. Coating L3 displays a high $|Z|_{0.01 \text{ Hz}}$ value with purely capacitive behavior after 2 h and does not show any change even after 7 days constant immersion in 5 wt% NaCl, indicating its excellent barrier performance. Coatings L1 and L2 displayed impedance much lower than L3, with $|Z|_{0.01 \text{ Hz}}$ values of around three orders of magnitude lower than L3 after immersion.

The barrier effect can also be explained by the observed T_g of the coatings (Table 5), apart from the NPH effect. The higher the wet T_g , the higher the barrier performance of the coating. The wet T_g was determined by soaking the coating film in electrolyte overnight and performing DSC on the wet film. Dry T_g was obtained by performing DSC on the dry sample.

As observed in Tables 3 and 5, coating L3 possessed the highest NPH, the highest EEW, and the highest T_g . The higher EEW indicated the lower amine require-

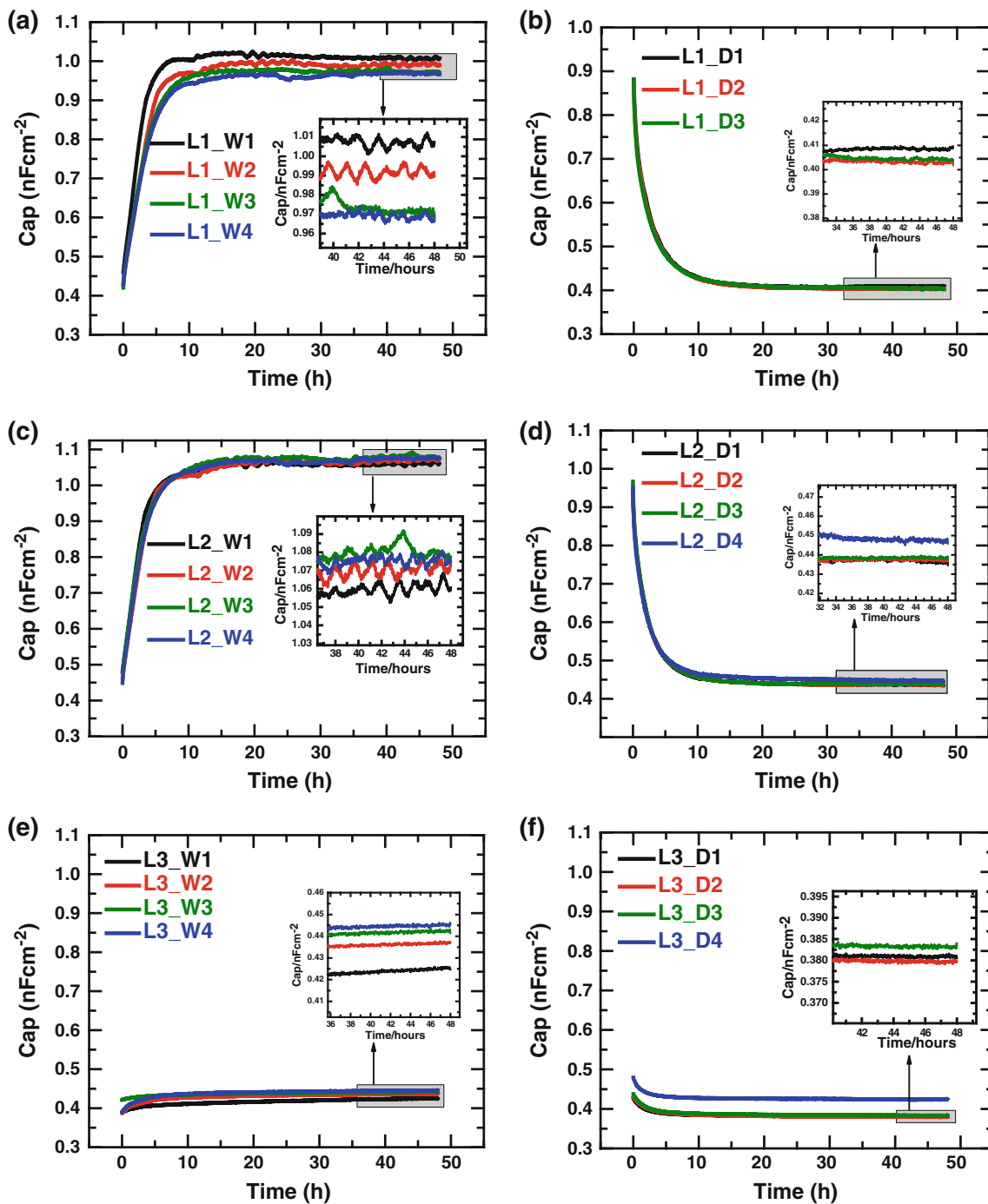


Fig. 14: Cycles of capacitance as a function of immersion time for coatings (a) L1 during wetting, (b) L1 during drying, (c) L2 during wetting, (d) L2 during drying, (e) L3 during wetting, and (f) L3 during drying. Some portions are magnified only to facilitate distinction of plots. However, comparison among the magnified regions cannot be made since their scales are different

ment for crosslinking and lower extent of generation of hydrophilic groups such as hydroxyl and tertiary amine during crosslinking (epoxy-amine reactions), resulting

in increased impedance. Thus, the higher impedance of the L3 coating is apparently determined by its associated NPH, EEW, and T_g .²²

Coating stability characterization by cyclic wetting–drying single frequency EIS capacitance measurement

Similar cyclic SF-EIS measurement was performed for the L series GC coatings, L1, L2, and L3. The fourth drying cycle for coating L1 could not be performed due to instrumental problems at the time of measurement.

The capacitance behavior shown in Fig. 14 reveals important information. In the wetting step, coatings L2 and L3 display similar capacitance trends for all the cycles, but for coating L1, a slight decrease in the capacitance is observed after every cycle. This indicates changes in the coating's dielectric behavior due to water absorption which could change the coatings molecular structure, form new product, or change the molecular orientation due to water ingress into the film. These changes subsequently influence the water uptake behavior in progressive wetting steps.^{41,42} Coating plasticization can be observed from the decrease in T_g measured for wet coating samples as compared to their respective dry samples as seen in Table 5. The slight decrease in the capacitance behavior of coating L1 after every cycle compared to coatings L2 and L3 indicates that coatings L2 and L3 are more stable compared to coating L1.

Conclusions

The effect of the polymer structure and composition on the EIS response of coatings was studied. It was shown that polymer structure and composition significantly control the electrochemical properties of the coating films cast from the polymers. The conclusions were as follows:

M series coatings: Coatings possessing the greatest hydrophilic group content in the polymer displayed the highest capacitance due to water uptake, whereas those having the greatest hydrophobic group content resisted water absorption. The water diffusion rate/diffusion coefficient also followed a similar trend. Changes in hydrophilic content in the polymer resulted in the change in capacitance behavior, an increase in hydrophilic content increasing the water uptake. The impedance behavior of the coating correlated with the EEW of the polymer, though a linear trend was not observed. SF-EIS was shown to have utility in testing for coating stability in wet-dry cycling.

L series coatings: An influence of polymer structure on the electrochemical behavior of coatings was observed. NPH content and EEW correlated well with the capacitance of the coating as well as with the rate of water uptake under immersion in 5% NaCl. Wet T_g of the coatings correlated with the impedance of the coatings. SF-EIS again can be used to test for coating stability.

The work reported in this paper has significant implications regarding the methodologies used to design

new polymer binder systems for high performance coatings. The preparation of a well-designed series of polymer binders having systematic variations in composition, characterization of the physical and mechanical properties of the binders, coupled with assessment of barrier properties using electrochemical methods as discussed herein, can result in a comprehensive picture of the structure–property relationships in the binder system. Simple water uptake measurements in electrolyte immersion, as is done here, can give excellent supplemental data to other lab tests. Moreover, information from this work can be used to optimize polymer composition for the specific performance properties needed in the application, saving significant time and effort in the research and development stage.

Acknowledgments The authors would like to thank the U.S. Army, Air Force, and National Energy Technology Laboratory (NETL) for funding this work.

References

1. Rao, AV, Kanitkar, DS, Parab, AK, “Some Speciality Coatings from Radiation Curable Poly(acrylic) Combinations.” *Prog. Org. Coat.*, **25** 221–233 (1995)
2. Wicks, ZW, Jones, FN, Pappas, SP, Wicks, DA, *Organic Coatings: Science and Technology*. Wiley-Interscience, New York, 2007
3. Edwards, PA, Striemer, G, Webster, DC, “Synthesis, Characterization and Self-crosslinking of Glycidyl Carbamate Functional Resins.” *Prog. Org. Coat.*, **57** 128–139 (2006)
4. Melchior, M, Sonntag, M, Kobusch, C, Jürgens, E, “Recent Developments in Aqueous Two-Component Polyurethane (2K-PUR) Coatings.” *Prog. Org. Coat.*, **40** 99–109 (2000)
5. Ravindran, N, Chattopadhyay, DK, Zakula, A, Battocchi, D, Webster, DC, Bierwagen, GP, “Thermal Stability of Magnesium-Rich Primers Based on Glycidyl Carbamate Resins.” *Polym. Degrad. Stab.*, **95** 1160–1166 (2010)
6. Edwards, PA, Striemer, G, Webster, DC, “Novel Polyurethane Coating Technology Through Glycidyl Carbamate Chemistry.” *J. Coat. Technol. Res.*, **2** 517–527 (2005)
7. Harkal, U, Muehlberg, A, Li, J, Garrett, J, Webster, D, “The Influence of Structural Modification and Composition of Glycidyl Carbamate Resins on Their Viscosity and Coating Performance.” *J. Coat. Technol. Res.*, **7** 531–546 (2010)
8. Deveci, H, Ahmetli, G, Ersoz, M, Kurbanli, R, “Modified Polystyrenes: Corrosion, Physicomechanical and Thermal Properties Evaluation.” *Prog. Org. Coat.*, **73** 1–7 (2012)
9. Rodríguez, MT, Gracenea, JJ, García, SJ, Saura, JJ, Suay, JJ, “Testing the Influence of the Plasticizers Addition on the Anticorrosive Properties of an Epoxy Primer by Means of Electrochemical Techniques.” *Prog. Org. Coat.*, **50** 123–131 (2004)
10. Li, J, Jeffcoate, CS, Bierwagen, GP, Mills, DJ, Tallman, DE, “Thermal Transition Effects and Electrochemical Properties in Organic Coatings: Part 1—Initial Studies on Corrosion Protective Organic Coatings.” *Corrosion*, **54** 763–771 (1998)
11. Kehr, J, *Fusion-Bonded Epoxy (FBE): A Foundation for Pipeline Corrosion Protection*. NACE International, Houston, 2003

12. Bierwagen, G, Jeffcoate, C, Li, J, Balbyshev, S, Tallman, D, Mills, D, “The Use of Electrochemical Noise Methods (ENM) to Study Thick, High Impedance Coatings.” *Prog. Org. Coat.*, **29** 21–29 (1996)
13. Bierwagen, G, “The Physical Chemistry of Organic Coatings Revisited—Viewing Coatings as a Materials Scientist.” *J. Coat. Technol. Res.*, **5** 133–155 (2008)
14. Mansfeld, F, Han, LT, Lee, CC, Zhang, G, “Evaluation of Corrosion Protection by Polymer Coatings Using Electrochemical Impedance Spectroscopy and Noise Analysis.” *Electrochim. Acta*, **43** 2933–2945 (1998)
15. Kern, P, Baner, A, Lange, J, “Electrochemical Impedance Spectroscopy as a Tool for Investigating the Quality and Performance of Coated Food Cans.” *J. Coat. Technol.*, **71** 67–74 (1999)
16. Oliveira, CG, Ferreira, MGS, “Ranking High-Quality Paint Systems Using EIS. Part I: Intact Coatings.” *Corros. Sci.*, **45** 123–138 (2003)
17. De Rosa, RL, Earl, DA, Bierwagen, GP, “Statistical Evaluation of EIS and ENM Data Collected for Monitoring Corrosion Barrier Properties of Organic Coatings on Al-2024-T3.” *Corros. Sci.*, **44** 1607–1620 (2002)
18. Mansfeld, F, “Use of Electrochemical Impedance Spectroscopy for the Study of Corrosion Protection by Polymer Coatings.” *J. Appl. Electrochem.*, **25** 187–202 (1995)
19. Gui, F, Kelly, R, “Performance Assessment and Prediction of Corrosion Prevention Compounds with Electrochemical Impedance Spectroscopy.” *Corrosion*, **61** 119–129 (2005)
20. Hinderliter, BR, Croll, SG, Tallman, DE, Su, Q, Bierwagen, GP, “Interpretation of EIS Data from Accelerated Exposure of Coated Metals Based on Modeling of Coating Physical Properties.” *Electrochim. Acta*, **51** 4505–4515 (2006)
21. Allahar, KN, Battocchi, D, Orazem, ME, Bierwagen, GP, Tallman, DE, “Modeling of Electrochemical Impedance Data of a Magnesium-Rich Primer.” *J. Electrochem. Soc.*, **155** E143–E149 (2008)
22. Harkal, U, Muehlberg, A, Webster, D, “Linear Glycidyl Carbamate (GC) Resins for Highly Flexible Coatings.” *J. Coat. Technol. Res.*, **10** 141–151 (2013)
23. Bierwagen, GP, Tallman, DE, “Choice and Measurement of Crucial Aircraft Coatings System Properties.” *Prog. Org. Coat.*, **41** 201–216 (2001)
24. Allahar, KN, Bierwagen, GP, Gelling, VJ, “Understanding AC–DC–AC Accelerated Test Results.” *Corros. Sci.*, **52** 1106–1114 (2010)
25. Bierwagen, G, Allahar, K, Hinderliter, B, Simões, AMP, Tallman, D, Croll, S, “Ionic Liquid Enhanced Electrochemical Characterization of Organic Coatings.” *Prog. Org. Coat.*, **63** 250–259 (2008)
26. Allahar, KN, Hinderliter, BR, Bierwagen, GP, Tallman, DE, Croll, SG, “Cyclic Wet Drying of an Epoxy Coating Using an Ionic Liquid.” *Prog. Org. Coat.*, **62** 87–95 (2008)
27. Simoes, A, Tallman, D, Bierwagen, G, “Use of Ionic Liquids for the Electrochemical Characterization of Water Transport in Organic Coatings.” *Electrochem. Solid-State Lett.*, **8** B60 (2005)
28. Hinderliter, BR, Allahar, KN, Bierwagen, GP, Tallman, DE, Croll, SG, “Thermal Cycling of Epoxy Coatings Using Room Temperature Ionic Liquids.” *J. Electrochem. Soc.*, **155** C93–C100 (2008)
29. Brasher, DM, Kingsbury, AH, “Electrical Measurements in the Study of Immersed Paint Coatings on Metal. I. Comparison Between Capacitance and Gravimetric Methods of Estimating Water Uptake.” *J. Appl. Chem.*, **4** 62–72 (1954)
30. Su, Q, Allahar, KN, Bierwagen, GP, “Application of Embedded Sensors in the Thermal Cycling of Organic Coatings.” *Corros. Sci.*, **50** 2381–2389 (2008)
31. Grundmeier, G, Schmidt, W, Stratmann, M, “Corrosion Protection by Organic Coatings: Electrochemical Mechanism and Novel Methods of Investigation.” *Electrochim. Acta*, **45** 2515–2533 (2000)
32. Allahar, KN, Hinderliter, BR, Simoes, AM, Tallman, DE, Bierwagen, GP, Croll, SG, “Simulation of Wet–Dry Cycling of Organic Coatings Using Ionic Liquids.” *J. Electrochem. Soc.*, **154** F177–F185 (2007)
33. Wind, MM, Lenderink, HJW, “A Capacitance Study of Pseudo-fickian Diffusion in Glassy Polymer Coatings.” *Prog. Org. Coat.*, **28** 239–250 (1996)
34. Lindqvist, S, “Theory of Dielectric-Properties of Heterogeneous Substances Applied to Water in a Paint Film.” *Corrosion*, **41** 69–75 (1985)
35. Bellucci, F, Nicodemo, L, “Water Transport in Organic Coatings.” *Corrosion*, **49** 235–247 (1993)
36. van Westing, EPM, Ferrari, GM, de Wit, JHW, “The Determination of Coating Performance with Impedance Measurements—II. Water Uptake of Coatings.” *Corros. Sci.*, **36** 957–977 (1994)
37. Mikovi-Stankovi, VB, Maksimovi, MD, Kaarevi-Popovi, Z, Zotovi, JB, “The Sorption Characteristics and Thermal Stability of Epoxy Coatings Electrodeposited on Steel and Steel Electrochemically Modified by Fe–P Alloys.” *Prog. Org. Coat.*, **33** 68–75 (1998)
38. Miskovic-Stankovic, VB, Drazic, DM, Kacarevic-Popovic, Z, “The Sorption Characteristics of Epoxy Coatings Electrodeposited on Steel During Exposure to Different Corrosive Agents.” *Corros. Sci.*, **38** 1513–1523 (1996)
39. Bierwagen, GP, He, L, Li, J, Ellingson, L, Tallman, DE, “Studies of a New Accelerated Evaluation Method for Coating Corrosion Resistance—Thermal Cycling Testing.” *Prog. Org. Coat.*, **39** 67–78 (2000)
40. Bethencourt, M, Botana, FJ, Cano, MJ, Osuna, RM, Marcos, M, “Lifetime Prediction of Waterborne Acrylic Paints with the AC–DC–AC Method.” *Prog. Org. Coat.*, **49** 275–281 (2004)
41. Bierwagen, G, Tallman, D, Li, J, He, L, Jeffcoate, C, “EIS Studies of Coated Metals in Accelerated Exposure.” *Prog. Org. Coat.*, **46** 149–158 (2003)
42. Chang, YP, Cheah, PB, Seow, CC, “Plasticizing—Antiplasticizing Effects of Water on Physical Properties of Tapioca Starch Films in the Glassy State.” *J. Food Sci.*, **65** 445–451 (2000)